25th ABCM International Congress of Mechanical Engineering
October 20-25, 2019, Uberlândia, MG, Brazil

COB-2019-0312
VORTEX IDENTIFICATION AND HEMODYNAMICS PATTERNS IN THE ASCENDING AORTA DURING A CARDIAC CYCLE OF A PATIENT-SPECIFIC PHANTOM

I. Ibanez
Pontifícia Universidade Católica do Rio de Janeiro, Department of Mechanical Engineering, 22451-900, Rio de Janeiro, RJ, Brazil
ing.aguilar04@gmail.com

B. A. de Azevedo
Pontifícia Universidade Católica do Rio de Janeiro, Department of Mechanical Engineering, 22451-900, Rio de Janeiro, RJ, Brazil
Instituto Nacional de Cardiologia - MS, Rio de Janeiro, RJ, Brazil
azevedo@puc-rio.br

A. O. Nieckele
Pontifícia Universidade Católica do Rio de Janeiro, Department of Mechanical Engineering, 22451-900, Rio de Janeiro, RJ, Brazil
nieckele@puc-rio.br

Abstract. *The main goal of this study is to numerically investigate hemodynamic patterns and coherent structures (vortex) during a complete cardiac cycle in the ascending aorta and aortic arch of a particular patient, who had an artificial valve implanted since he suffered of an aortic stenosis. A 3D model was generated from computed tomography angiography and image segmentation of the ascending aorta and aortic arch. The boundary conditions were defined based on physiological bloody pressure and mass flow rates entering and leaving the aorta, respectively. The turbulence was modeled with the two-equation κ–ω SST model. The geometrical vortex shape evolution in the cardiac cycle is discussed and the effect of blood flow on the aortic wall during the cardiac cycle is analyzed through the wall shear stress (WSS) distribution. Finally, it is shown that the vortex shape and the vortex location may have a relationship with the regions of high WSS.*

Keywords: *Vortex, Wall Shear Stress, CFD, Aortic stenosis, Cardiac cycle*

1. INTRODUCTION

Cardiovascular diseases cause the greatest number of deaths in the world. According to the World Health Organization (WHO) 17.9 million people died during 2016 as a result of any cardiovascular disease, totalizing 31% of total deaths in the world. Aortic stenosis is one of the most severe cardiovascular pathologies. Aortic stenosis is a condition characterized by narrowing, hardening, thickening, fusion or blockage of the aortic valve. A significant stenosis produces a pressure overload in the left ventricle. As a result of increased pressure, the myocardium is subjected to hypertrophy, and this can lead to heart failure (Mohler *et al.*, 1991). Aortic stenosis may cause a modification in the blood trajectory within the aorta and an increase of the WSS in the region of the ascending aorta (Celis *et al.*, 2017; Gomes *et al.*, 2017).

In relation to the hemodynamic changes caused by the aortic stenosis, the analysis of coherent structures (vortices) is relevant and the knowledge of these structures may help understand why the disease develops. Callaghan *et al.* (2015) by using Criterion λ was able to estimate the location and intensity of the vortices within an aortic arch aneurysm. Gilmanov e Sotiropoulos (2016), using Criterion Q, presented a comparison between the vortex structures in the aortic root generated from a healthy tricuspid aortic valve and a bicuspid aortic valve. Wald *et al* (2018) analyzed the vortex location in the aortic root with different configurations of the aortic valve (healthy and stenotic). Criterion λ (Jeong e Hussain, 1995) and Criterion Q (Hunt *et al.*, 1988) are mathematical strategies that relate the strain tensor and the rotational tensor in order to identify the existence of vortex structures.

The main objective of this study is to numerically identify vortex structures (Criterion Q) and hemodynamic patterns within the ascending aorta and aortic arch during a complete cardiac cycle of a patient, who presented a stenosis aortic and had an artificial valve implanted. The wall shear stress WSS distribution in the region of the ascending aorta and aortic arch is also discussed.

2. METODOLOGY

Aiming to analyze the flow field inside an aorta of a specific patient, a computational domain must be created. To this end, medical images were obtained using a computed tomography angiography. Use of this specific patient images was

approved by the board of the National Institute of Cardiology (INC) of Rio de Janeiro. Aorta segmentation process was completed using FIJI (open source image processing software based on ImageJ) and the computational domain illustrated in Fig. 1 was created in the ICEM-CFD tool of the ANSYS package, version 18.

The flow enters the aorta through the aortic valve from the heart. Four outlet section were considered, three through the aorta´s arch near the brachiocephalic trunk and the main outlet at the descending side of the aorta, Fig.1.

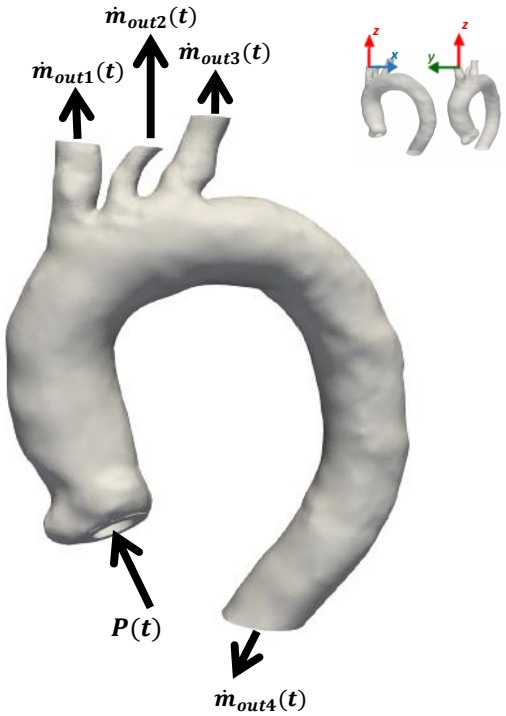

Figure 1. Computational domain, with schematization of the boundary conditions for a cardiac cycle.

To model the blood flow through the aorta, the following hypotheses were considered:

(i) isothermal flow since the temperature gradients are small (Hao, 2010);
(ii) the blood is considered as incompressible, given the typical pressure variations found in large arteries (Feijóo e Zouain, 1988; Li, 2004);
(iii) negligible gravitational effects;
(iv) turbulent blood flow (Davies *et al.*, 1986; Celis *et al.*, 2017; Gomes et al, 2017);
(v) the aortic blood flow can be considered as Newtonian fluid with constant viscosity, this is a valid approximation for strain rates higher than 50 s^{-1} (Stuart e Kenny, 1980; Long *et al.*, 2004; Crowley e Pizziconi, 2005), as obtained in this work;
(vi) the aorta surface was considered rigid as suggested by Jin *et al.* (2003).
(vii) aorta valve is a circular orifice with the effective diameter
(viii) negligible flow through the right coronary, near the inlet

The blood flow was determined by the solution of the time average mass and momentum conservation equations, Eqs. (1) and (2), employing ANSYS Fluent software.

$$\frac{\partial u_i}{\partial x_i} = 0 \tag{1}$$

$$\frac{\partial\, \rho\, u_i}{\partial t} + \frac{\partial \rho\, u_j\, u_i}{\partial x_j} = -\frac{\partial\, \hat{p}}{\partial x_i} + \frac{\partial}{\partial x_j}\left\{(\mu + \mu_t)\, 2\, S_{ij}\right\} \tag{2}$$

where x_i represents each of the coordinate axes and u_i the components of the velocity vector, ρ is the density, μ is the molecular viscosity, μ_t is the turbulent viscosity and $\hat{p}$ is a modified pressure that includes the turbulent dynamic pressure (based on the turbulent kinetic energy κ) and is given by:

$$\hat{p} = p + \frac{2}{3}\rho\, \kappa \tag{3}$$

S_{ij} is the rate of deformation tensor

$$S_{ij} = \frac{1}{2}\left(\frac{\partial u_i}{\partial x_j} + \frac{\partial u_j}{\partial x_i}\right) \tag{4}$$

To model the turbulence, the κ-ω SST turbulence model (Menter, 1994).was selected. This model was chosen based on the research developed by Celis *et al* (2017), who studied the performance of several turbulent models to predict the flow in the ascending aorta, and showed that the κ-ω SST model presented good agreement when compared to the experimental data of Gomes *et al.* (2017). This model combines the robust and accurate formulation of the κ-ω model in the region close to the wall with the free-flow independence of the κ-ε model in the distant field. According with the κ-ω SST model, the turbulent viscosity is computed from:

$$\mu_t = \frac{\rho\kappa}{\omega}\,\xi \tag{5}$$

where ξ is a blending factor of the $\kappa - \varepsilon$ with the $\kappa - \omega$ model. The kinetic energy κ and specific rate of dissipation ω were calculated from the solution of their conservation equations, available in ANSYS Fluent software

A periodic cardiac cycle of 1 second was considered. The boundary conditions were defined based on a physiological pressure profile in the inlet (Crosetto *et al.*, 2011; Reymond *et al.*, 2013) as shown in Fig. 2, with turbuent intensity equal to 5% based on recommendation of Gomes (2017) and Cellis (2017). The inlet specific rate of dissipation was determined based on a characteristic length ℓ equal to $0.07D$, where D is the valve effective diameter. At each of the outlet indicted in Fig. 1, the physiological mass flow profile (Alastruey *et al.*, 2016) shown in Fig. 3 were imposed.

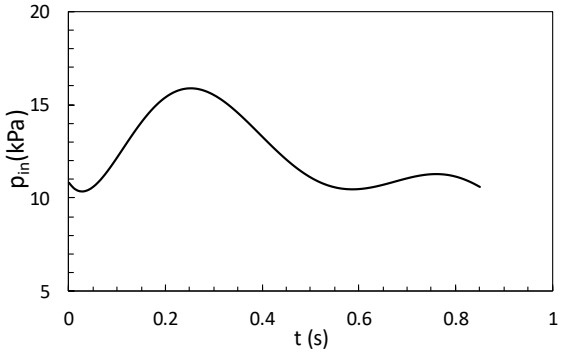

Figure 2. Pressure profile in the inlet

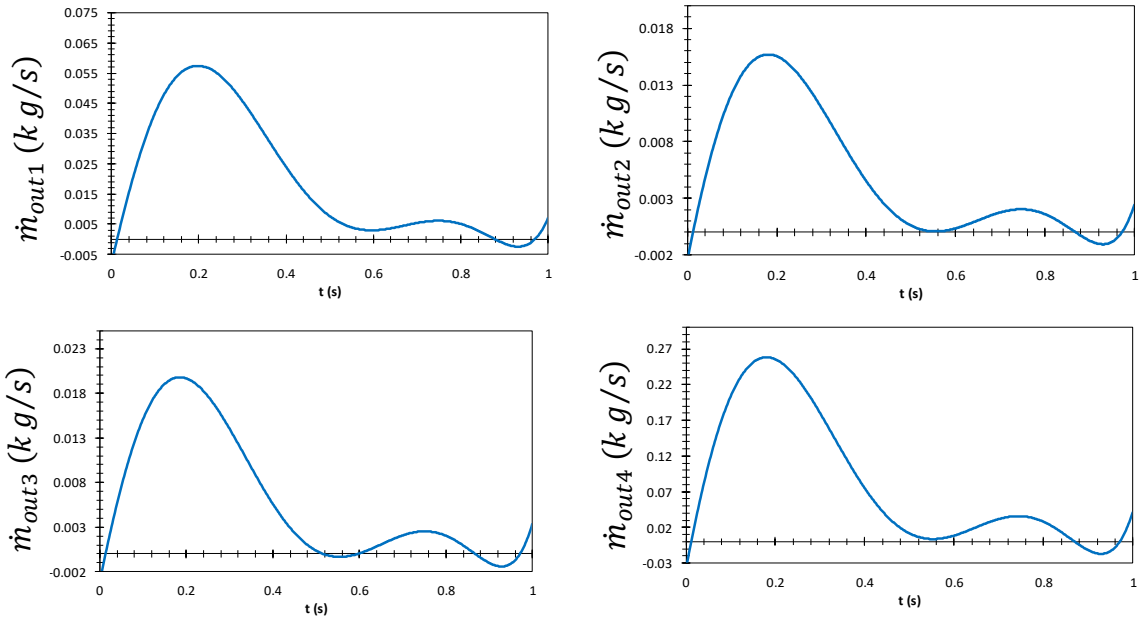

Figure 3. Mass flow profile in each one of the outputs.

Inside the computational domain, a mesh of tetrahedral elements was constructed. To define the mesh a rigorous spatial resolution test was performed. The mesh selected to perform the CFD simulations had 2 million elements, based

on variation inferior to 0.5% for the wall pressure and 2% for the wall shear stress, after doubling the number of elements.

The flow field was determined during 5 cycles. It was observed that after three cycles a periodic solution had been attained. However, to guarantee a periodic solution, the flow field was examined during the fifth cycle.

3. RESULTS AND DISCUSION

Hemodynamic effects and vortex structures were studied through the analysis of wall shear stress (WSS) and criterion Q . Hunt *et al.* (1988) defines criterion Q as:

$$Q = \frac{1}{2}\left(\Omega_{ij}\Omega_{ij} - S_{ij}S_{ij}\right) \tag{6}$$

where Ω_{ij} is the rotational tensor

$$\Omega_{ij} = \frac{1}{2}\left(\frac{\partial u_i}{\partial x_j} - \frac{\partial u_j}{\partial x_i}\right) \tag{7}$$

and S_{ij} is the strain tensor (or rate of deformation tensor), Eq. (4). Vortices can appear in the regions of the domain where $Q > 0$ since this implies that the rotational tensor is dominant over the strain tensor.

At different time instants of the cardiac cycle, Figure 4 shows a Q criterion isosurface (3000 s^{-2}). Six time instants were selected to be examined. For each time instant, two views of the aorta are presented in Fig. 4 to aid the interpretation of the flow. To complement the information regarding the intensity of the vortex, they are colored by the magnitude of vorticity ξ over it, where

$$\xi = \sqrt{2\,\Omega_{ij}\Omega_{ij}} \tag{8}$$

Finally, an isosurface of the velocity magnitude (1 m/s, red color) is also shown in Figure 4, which represents the velocity jet contour.

Analyzing Figure 4, the following behaviors regarding to the coherent structures were identified:

(i) until 0.10 s the vortex has a toroidal geometric contour and it is located in the velocity jet periphery;
(ii) between the time instant of 0.15 s and 0.25 s the vortex geometric shape turns from toroidal into a hairpin, in this period of time the vortex continues proximal to the velocity jet;
(iii) from the time instants of 0.30 s it is observed how the hairpin vortex begins to be subdivided into small vortices, this can be understood as a consequence of the velocity jet impact in the wall and
(iv) at time instant of 0.35 s the velocity jet is practically faded and several of small vortices are visible.

Regarding to shear stress in the ascending aorta and aortic arch Figure 5 illustrates the WSS distribution for different time instants of the cardiac cycle. It is notice that at the beginning of the cycle (0.1 s) a more uniform distribution and lower values of WSS are observed. As the mass flow rate increases (0.2 s), in the wall region of the jet impact high values of WSS are obtained. At the end of the systole (0.3 s) and with the reduction of mass flow, the WSS decreases however there is still some region close to aortic arch with high WSS values. At the diastolic period (0.5 s) due to small velocity, the WSS is also low and becomes more uniform.

4. CONCLUSION

From the hemodynamic patterns it is observed that it is important to take into consideration the entire cardiac cycle in order to analyze the effect of blood flow on the aortic wall. It was noticed a possible relationship in terms of the geometrical form between the WSS uniformity in the aortic root and the toroidal shape of the vortex at the beginning of the systole. It was also observed that the region of high WSS seems to be related with the presence of vortex with hairpin shape at the maximum point of the systole. Finally, it was noted that the vortices spreading looks linked to the dispersion of high values of WSS at the end of the systole stage.

These hemodynamic behaviors may be relevant in the process of aortic remodeling, since the shape of the vortex and its location may lead to regions of high WSS.

5. ACKNOWLEDGEMENTS

This work was supported by the Cardiovascular Engineering Laboratory PUC-Rio. The authors also thank Brazilian government agencies CNPq and CAPES for the continuous support.

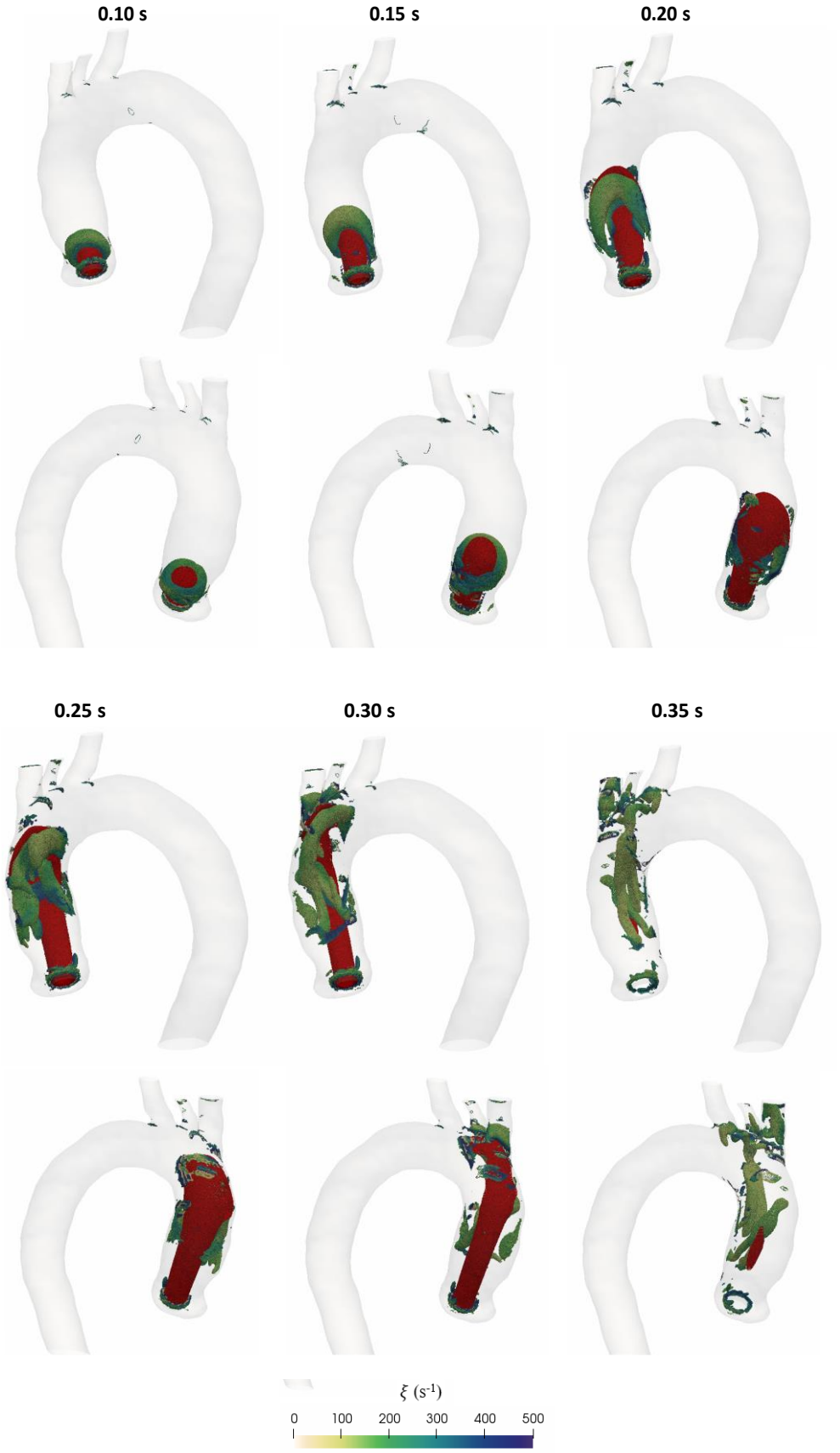

Figure 4. Vortex identification (Criterion Q); Magnitude of vorticity ξ (s^{-1}) and Velocity jet (1 m/s)

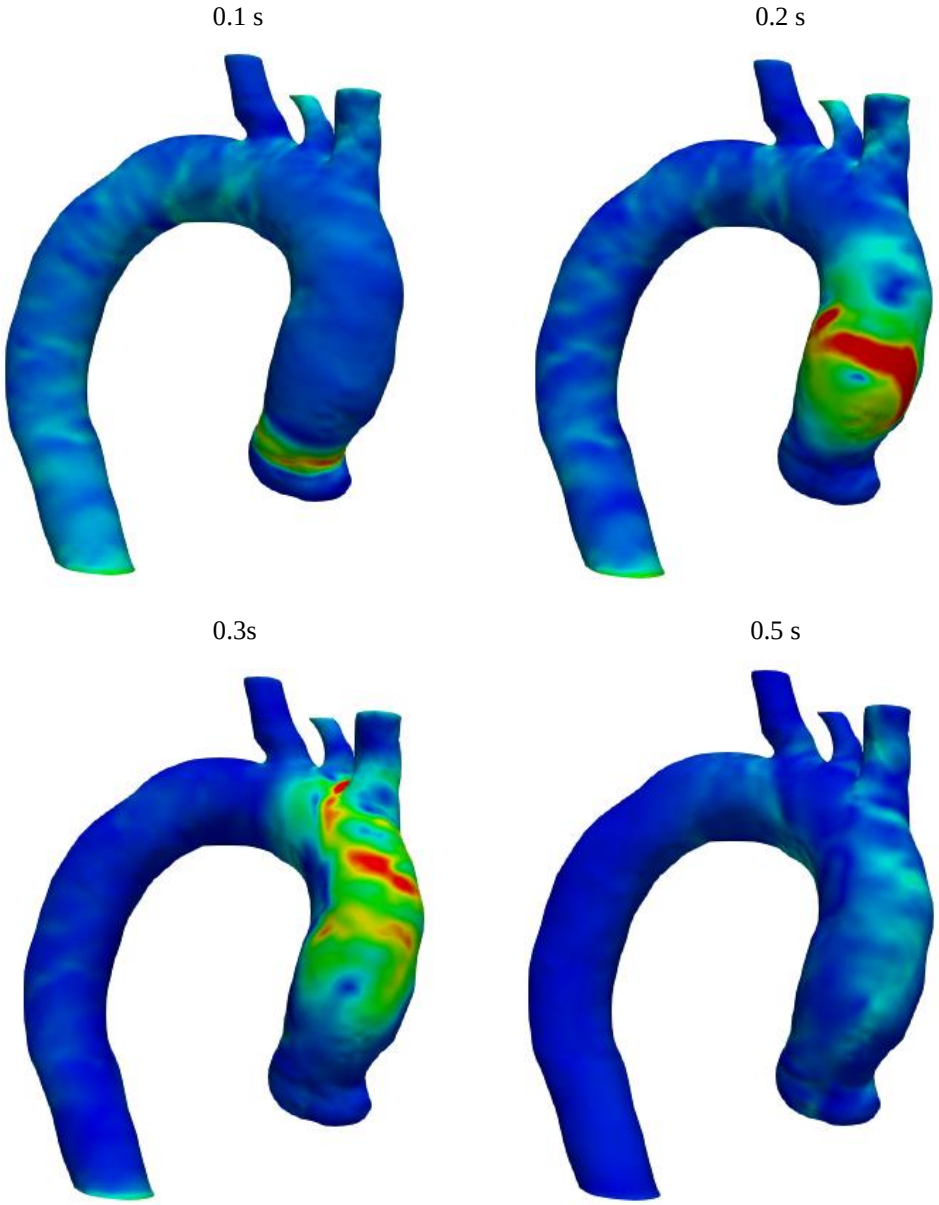

Figure 5. WSS at 0.1 s acceleration stage of systole); 0.2 s (maximum point of systole); 0.3 s (close to systole end) and 0.5 s (diastole stage)

6. REFERENCES

Alastruey, J., Xiao, N., Fok, H., Schaeffter, T., & Figueroa, C. A. (2016). On the impact of modelling assumptions in multi-scale, subject-specific models of aortic haemodynamics. *Journal of The Royal Society Interface, 13*(119), 20160073.

Callaghan, F., Karkouri, J., Broadhouse, K., Evin, M., Fletcher, D., & Grieve, S. (2015). Thoracic aortic aneurysm: 4D flow MRI and computational fluid dynamics model. *Computer methods in biomechanics and biomedical engineering, 18*(sup1), 1894-1895.

Celis, D., Ibañez, I., Nieckele Azevedo, P., Nieckele , A., & Gomes, B. (2017). *Numerical investigation of hemodynamics patterns after Transcatheter Aortic Valve Replacement (TAVR)*. Proc. 24th ABCM International Congress of Mechanical Engineering, Curitiba.

Crosetto, P., Reymond, P., Deparis, S., Kontaxakis, D., Stergiopulos, N., & Quarteroni, A. (2011). Fluid–structure interaction simulation of aortic blood flow. *Computers & Fluids, 43*(1), 46-57.

Crowley, T. A., & Pizziconi, V. (2005). Isolation of plasma from whole blood using planar microfilters for lab-on-a-chip applications. *Lab on a Chip, 5*(9), 922-929.

Davies, P. F., Remuzzi, A., Gordon, E. J., Dewey, C. F., & Gimbrone, M. A. (1986). Turbulent fluid shear stress induces vascular endothelial cell turnover in vitro. *Proceedings of the National Academy of Sciences, 83*(7), 2114-2017.

Feijóo, R., & Zouain, N. (1988). Formulations in rates and increments for elastic-plastic analysis. *International Journal for numerical methods in engineering, 26*(9), 2031-2048.

Gilmanov, A., & Sotiropoulos, F. (2016). Comparative hemodynamics in an aorta with bicuspid and trileaflet valves. *Theoretical and Computational Fluid Dynamics, 30*(1-2), 67-85.

Gomes, B. A. d. A., Camargo, G. C., Santos, J. R. L. d., Azevedo, L. F. A., Nieckele, Â. O., Siqueira-Filho, A. G., & Oliveira, G. M. M. d. (2017). Influence of the tilt angle of Percutaneous Aortic Prosthesis on Velocity and Shear Stress Fields. *Arquivos Brasileiros de Cardiologia, 109*(3), 231-240.

Hao, Q. (2010). Modeling of Flow in an In Vitro Aneurysm Model: A Fluid-Structure Interaction Approach. Dissertation. University of Miami.

Hunt, J. C., Wray, A. A., & Moin, P. (1988). Eddies, streams, and convergence zones in turbulent flows. *Proceedinngs. Summer Program*, Center for Turbulence Research

Jin, S.; Oshinski, J.; Giddens, D.P. Effects of wall motion and compliance on flow patterns in the ascending aorta. *Journal of Biomechanical Engineering*, 125(3), 347-354, 2003.

Jeong, J., & Hussain, F. (1995). On the identification of a vortex. *Journal of fluid mechanics, 285*, 69-94.

Li, J. K. (2004). *Dynamics of the vascular system* (Vol. 1): World scientific.

Long, D. S., Smith, M. L., Pries, A. R., Ley, K., & Damiano, E. R. (2004). Microviscometry reveals reduced blood viscosity and altered shear rate and shear stress profiles in microvessels after hemodilution. *Proceedings of the National Academy of Sciences, 101*(27), 10060-10065.

Menter, F. R. (1994). Two-equation eddy-viscosity turbulence models for engineering applications. *AIAA journal, 32*(8), 1598-1605.

Mohler, E. R., Nichols, R., Harvey, W., Sheridan, M., Waller, B., & Waller, B. F. (1991). Development and progression of aortic valve stenosis: atherosclerosis risk factors—a causal relationship? A clinical morphologic study. *Clinical cardiology, 14*(12), 995-999.

Reymond, P., Crosetto, P., Deparis, S., Quarteroni, A., & Stergiopulos, N. (2013). Physiological simulation of blood flow in the aorta: comparison of hemodynamic indices as predicted by 3-D FSI, 3-D rigid wall and 1-D models. *Medical Engineering and Physics, 35*(6), 784-791.

Stuart, J., & Kenny, M. W. (1980). Blood rheology. *Journal of clinical pathology, 33*(5), 417.

Wald, S., Liberzon, A., & Avrahami, I. (2018). A numerical study of the hemodynamic effect of the aortic valve on coronary flow. *Biomechanics and modeling in mechanobiology, 17*(2), 319-338.

7. RESPONSIBILITY NOTICE

The authors are the only responsible for the printed material included in this paper.